First published online as a Review in Advance on November 7, 2007

Molecular Ordering and Phase Behavior of Surfactants at Water-Oil Interfaces as Probed by X-Ray Surface Scattering

Mark L. Schlossman[1] and Aleksey M. Tikhonov[2]

[1]Departments of Physics and Chemistry, University of Illinois at Chicago, Chicago, Illinois 60607; email: schloss@uic.edu

[2]Center for Advanced Radiation Sources, University of Chicago, and Brookhaven National Laboratory, National Synchrotron Light Source, Upton, New York 11973

Annu. Rev. Phys. Chem. 2008. 59:153–77

The *Annual Review of Physical Chemistry* is online at http://physchem.annualreviews.org

This article's doi: 10.1146/annurev.physchem.59.032607.093822

0066-426X/08/0505-0153$20.00

Key Words

liquid-liquid, monolayers, multilayers, inhomogeneous phases, X-ray reflectivity

Abstract

Surfactants have their primary utility, both scientific and industrial, at the liquid-liquid interface. We review recent X-ray surface scattering experiments that probe the molecular ordering and phase behavior of surfactants at the water-oil interface. The presence of the oil modifies the interfacial ordering in a manner that cannot be understood simply from analogies with studies of Langmuir monolayers of surfactants at the water-vapor interface or from the traditional view that the solvent is fully mixed with the interfacial surfactants. These studies explored the role of chain flexibility and head group interactions on the ordering of long-chain alkanols and alkanoic acids. Small changes in the surfactant may produce large changes in the interfacial ordering. The interfacial monolayer can be spatially homogeneous or inhomogeneous. Investigators have observed interfacial phase transitions as a function of temperature between homogenous phases, as well as between homogeneous and inhomogeneous phases. Finally, varying the solvent chain length can alter the fundamental character of the phase transitions and lead to the formation of multilayer interfacial structures.

1. INTRODUCTION

The scientific investigation and industrial utilization of surfactants are extensive, ongoing enterprises. Techniques such as X-ray and neutron surface scattering and nonlinear optics, which are specifically sensitive to surface phenomena, have contributed to these enterprises by determining the ordering and phase behavior of molecules at liquid-vapor interfaces (1–4) and, more recently, at water-oil interfaces (5, 6). In this review, we focus on scattering studies of single interfaces between macroscopically phase-separated water and oil phases, as opposed to scattering studies of bulk materials that probe the structure of internal interfaces owing to microscopic phase separation, such as those formed by micelles, microemulsions, and vesicles (7). We discuss primarily X-ray surface scattering studies, which have led recently to a new understanding of surfactant ordering at water-oil interfaces.

The surfactants of concern to us consist of polar head groups (e.g., alcohol, $–CH_2OH$, or carboxylic acid, –COOH) at the end of a long alkyl or partially fluorinated alkyl chain [$CH_3(CH_2)_{m-1}–$ with m varying from 20 to 30 or $CF_3(CF_2)_{m-3}(CH_2)_2–$ with $m = 10$ or 12]. These surfactants are soluble at low concentrations in hydrocarbon oils, such as alkane liquids (e.g., hexane). If a hexane solution of these surfactants is placed in contact with bulk water, the surfactants minimize their free energy by partitioning between the bulk hexane and the water-hexane interface. A surfactant that goes to the interface can lower its energy by positioning its polar head group in the polar environment of water, which may also allow for hydrogen bonding between its head group and water. However, the translational entropy of the surfactant is reduced. Also, water and hexane molecules that were formerly at the interface are displaced in this process.

As more surfactants are adsorbed to the interface, it is sensible to think that interactions between surfactants, such as repulsive steric and attractive van der Waals interactions, become important. However, in an influential textbook, Davies & Rideal (8) summarized earlier work by stating that "molecules of oil penetrate between the hydrocarbon chains and remove all interchain attractions," thus leading to the widely held views "that the $–CH_2–$ groups in the adsorbed film are free to move laterally" and that surfactant monolayers at the water-oil interface are more disordered than the corresponding monolayers at the water-vapor interface (9). Pethica and coworkers (10, 11) discussed similar ideas in their experimental studies of lipids at the water-oil interface.

Recent X-ray results have contradicted this point of view, for example, by demonstrating the presence of solid close-packed surfactant monolayers at water-oil interfaces (12–14). Interfacial tension measurements provided evidence for condensed monolayers without specifying whether they were solid or liquid (15–20). The formation of a solid monolayer may result from strong interactions between the surfactant chains that overcome the loss of entropy due to the conformational degrees of freedom of the chains. Therefore, a prime candidate for the formation of a solid monolayer is a surfactant whose chain is relatively rigid, such as the partially fluorinated alkanol $CF_3(CF_2)_{m-3}(CH_2)_2OH$ ($m = 10$ or 12) (12, 13). In this case, little conformational entropy is lost when these chains form a close-packed solid

monolayer at the water-hexane interface. Alternatively, we have also observed close-packed, nearly all-*trans* monolayers at the water-hexane interface of neutral alkanoic acids [$CH_3(CH_2)_{m-2}COOH$, $m = 18$, 20, and 30] that have flexible alkyl tails (14). However, it seems that just the van der Waals attractions of the chains alone are not enough to overcome the disordering effect of the tail conformational entropy. This is suggested by observations of monolayers of alkanol surfactants [$CH_3(CH_2)_{m-1}OH$, $m = 20$ to 30] at the water-hexane interface for which the most stable dense monolayer phase is a liquid with disordered tail groups (21, 22). Molecular dynamics simulations suggest that an additional attractive interaction (extensive hydrogen bonding of alkanoic acid head groups to their neighboring head groups), which is not present in the alkanol monolayers, is responsible for the formation of solid monolayers of the neutral alkanoic acids at the water-hexane interface (14).

These results support the view that the oil solvent has a strong influence on molecular ordering at the interface. Long chain alkanols form solid all-*trans* monolayers at the water-vapor interface (22–25), although they form liquid monolayers with disordered tails at the water-hexane interface (21, 22). A small amount of hexane penetrating the region of the monolayer is possible, and our measurements place an upper bound on the amount, but not a lower bound (22). Here, the oil solvent has acted to disorder the monolayer, although perhaps not exactly as envisioned by Davies & Rideal (8). Surprisingly, even changing the chain length of the alkane solvent (e.g., from hexane to hexadecane) can greatly alter an adsorbed surfactant layer (26). As shown below, this particular change can alter the interfacial phase of tetracosanol [$CH_3(CH_2)_{23}OH$] from a monolayer to a multilayer (26).

In spite of the dissimilarities between surfactant layers at the water-oil interface and the corresponding layers of the same surfactants at the water-vapor interface, a further comparison is useful. Micrometer-scale domains of condensed monolayer phases are observed at both interfaces, and long-range dipole interactions likely stabilize these domains at both interfaces (27–30). The monolayers discussed in this article, at the water-oil interface, are in equilibrium owing to the exchange of surfactants between the interface and the bulk oil. Therefore, these monolayers are not easily overcompressed into a metastable or unstable state, as is the case with monolayers at the water-vapor interface. This has been used to an advantage at the water-vapor interface to study domain instabilities (31), but the issue of very long relaxations of internal degrees of freedom in solid monolayers, and their effect on the monolayer phase diagram, has not been fully resolved for Langmuir monolayers (32–34).

There is a striking dissimilarity between the phase diagrams of, say, long-chain alkanol monolayers at the water-oil and at the water-vapor interfaces. For an interface between water and an oil solution of a single surfactant, the interfacial phase is determined by the bulk pressure, temperature, and bulk concentration of the surfactant (15, 35–37). For adequately high temperatures, the interfacial phase appears to be a surfactant gas (22). As the temperature is lowered, a phase transition occurs at which the alkanols form a liquid monolayer phase (22). Depending on the particular chain length, domains may form en route to this transition (13, 22, 38). If, as Lyklema (39) has suggested, the equation of state is the same for these surfactants at the water-oil and water-vapor interfaces, then one might expect that further lowering the

temperature would produce a sequence of solid phases, varying in unit cell and tilt angle of the essentially all-*trans* tail group, as is observed for long-chain alkanols at the water-vapor interface when the surface pressure is increased (21, 23–25, 40–45). This is not the case. Instead, before a low-enough temperature is reached at which the liquid monolayer might undergo a transition to a solid monolayer, the alkanol precipitates out of the solution. Also, if the equations of state are the same, one expects the same interfacial monolayer phase for the same interfacial concentration of the surfactant (and temperature and bulk pressure). This is also not the case because the long-chain alkanols at the water-oil interface form only a liquid monolayer phase, whereas at the water-vapor interface they form a solid monolayer phase under similar conditions. This is true even for the same average interfacial density because the solid phase at the water-vapor interface forms a spatially inhomogeneous phase in which solid-phase domains are separated by interfacial regions of much lower surfactant density (23–25). In the sections below, we present evidence gathered from X-ray surface scattering, interfacial tension, and Brewster angle microscopy for many of the phenomena mentioned in this introduction.

2. X-RAY SURFACE SCATTERING METHODS

Two X-ray surface scattering techniques have proven useful in the study of surfactant layers at the water-oil interface—X-ray reflectivity and off-specular diffuse scattering, also known as grazing-incidence small-angle X-ray scattering (GISAXS) (1, 46, 47). X-ray reflectivity probes the variation of electron density with depth into the interface and by implication the molecular ordering with subnanometer resolution at water-oil interfaces. GISAXS can determine the average radius and separation of micrometer-scale domains in surfactant monolayers (38, 47). Both techniques are sensitive to the fraction of the interface covered by the monolayer phase. In addition to the studies of surfactant layers discussed here, researchers have recently used these X-ray techniques to study other phenomena at the liquid-liquid interface, including the structure of the neat interface (without surfactants) between water and alkane liquids of varying chain lengths (from 6 to 22 carbons long) (48, 49); the neat interface between water and polar oils such as 2-heptanone or nitrobenzene (50, 51); liquid-liquid interfaces between thin wetting films, including protein adsorption at this interface (52–56); the ordering of surfactant mixtures at the water-oil interface (57); phospholipid monolayers at the water-oil interface (58–60); the microemulsion-water interface (61–63); critical phenomena at the liquid-liquid interface (64); the ordering of nanoparticles at the water-oil interface (65, 66); the ordering of ions at the oil/silica hydrosol (66–69); and ion distributions at the electrified interface between two electrolyte solutions (51, 70, 71).

The scattering geometry for X-ray reflectivity shown in **Figure 1** indicates that X rays pass through the upper liquid phase on their way to the interface. Significant absorption of the X rays by the liquid and the need to adjust reflection angles on a millidegree scale dictate the use of a synchrotron X-ray source that can provide a highly collimated, intense, and relatively high-energy (typically 15 keV or higher) beam of X rays (72, 73). Reflectivity data are measured as a function of wave-vector transfer normal to the interface, $Q_z = (4\pi/\lambda)\sin\alpha$ when the in-plane components of

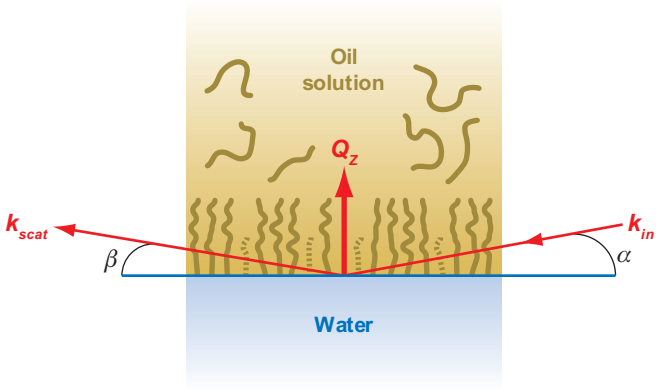

Figure 1

X-ray scattering geometry from the interface between water and an oil solution of surfactants. The X rays pass through the upper oil solution, then reflect off the surfactant monolayer at the interface. X-ray reflectivity is measured with $\alpha = \beta$ (equal incident and reflection angles). The wave-vector transfer for reflectivity, $Q_z = (4\pi/\lambda)\sin\alpha$, is normal to the interface, indicating that reflectivity probes structure normal to the interface. Off-specular diffuse scattering is measured by fixing α and scanning β, leading to a nonzero in-plane component of the wave-vector transfer and a sensitivity to in-plane structure.

the wave vector are set to zero. The X-ray wavelength λ is typically 0.825 Å, and the incident and reflected angles are equal for specular reflection ($\beta = \alpha$ in **Figure 1**) (12, 22, 73). Specular reflection probes structure normal to the interface, but averaged over the in-plane region of the interface.

One can analyze X-ray reflectivity $R(Q_z)$ from the water-oil interface to yield the electron density profile by using the first Born approximation, written as (46)

$$\frac{R(Q_z)}{R_F(Q_z)} \approx \left| \frac{1}{(\rho_W - \rho_O)} \int dz \frac{d\langle \rho_e(z)\rangle_{xy}}{dz} \exp(i\,Q_z z) \right|^2, \qquad (1)$$

where z is in the normal direction; $\langle \rho_e(z)\rangle_{xy}$ is the electron density profile averaged over the surface area of the interface illuminated by the X rays; ρ_W and ρ_O are the electron densities of bulk water and oil, respectively (e.g., $\rho_W = 0.3337\ e^-\ \text{Å}^{-3}$ and $\rho_{Hexane} = 0.230\ e^-\ \text{Å}^{-3}$ at $T = 20°\text{C}$); and the Fresnel reflectivity $R_F(Q_z)$ is calculated for an ideal interface at which the electron density changes abruptly from the value of one bulk phase to the other and is expressed as (74, 75)

$$R_F(Q_z) \approx \left| \frac{Q_z - Q_z^T}{Q_z + Q_z^T} \right|^2, \qquad (2)$$

where $Q_z^T = (Q_z^2 - Q_c^2)^{1/2}$ is the z component of the wave-vector transfer with respect to the lower phase. Equation 1 is accurate for $Q_z \geq 4Q_c$, where total reflection of X rays from the lower phase occurs for $Q_z \leq Q_c$, and the critical wave-vector transfer is $Q_c = 4(\pi r_e(\rho_W - \rho_O))^{1/2}$ ($\approx 0.012\ \text{Å}^{-1}$ for the water-hexane interface), where r_e is the classical electron radius. Although Equation 1 provides insight into the reflection process, the Parratt formalism is an alternative and exact method often used to analyze reflectivity measurements (76).

X-ray reflectivity is specifically sensitive to surface or interfacial structure (1). Equation 1 indicates that reflected X rays are produced when the electron density varies with depth into the interface. X rays passing through bulk liquid phases do not produce reflections because the value of the electron density, when averaged over the *x-y* plane, is constant with depth. Reflected X rays are produced when incident X rays encounter the top, or bottom, of a monolayer because the electron density changes with depth in those regions. Similarly, internal structure within the monolayer could produce reflected X rays. An example of this is the depth at which the head groups within an ordered surfactant monolayer are bound to the tail groups. These various reflections coherently interfere to produce the total X-ray reflectivity. One analyzes the shape and intensity of the interference fringes produced by the variation of reflectivity with wave-vector transfer Q_z (or, equivalently, incident angle) to yield the electron density variation with depth through the interface.

Figure 2*a* gives an example of such interference fringes, illustrating X-ray reflectivity data for alkanols $CH_3(CH_2)_{m-1}OH$ with $m = 20$, 22, 24, and 30 (22). These

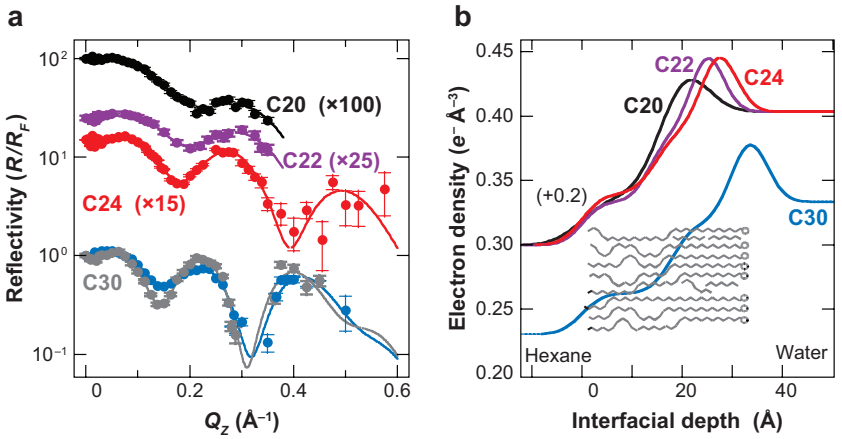

Figure 2

(*a*) X-ray reflectivity (normalized to the Fresnel reflectivity) as a function of the wave-vector transfer normal to the interface for *n*-alkanol monolayers at the water-hexane interface. At the chosen temperatures, the monolayers are in a condensed (liquid) monolayer phase [C*m* refers to $CH_3(CH_2)_{m-1}OH$]: C20 at 19.4°C, C22 at 21.6°C, C24 at 21.93°C, C30 (*gray*) at 24.1°C, and C30 (*blue*) at 24.5°C (see **Figure 4** for alkanol concentrations in hexane). Curves have been offset for clarity. Lines are fits described in the text. Two slab models are used for C20 and C22, whereas three slab models are used for C24 and C30. (*b*) Electron density profiles for alkanol monolayers at the water-hexane interface determined from the data shown in panel *a* (the profile for C30 at 24.5°C is shown). Profiles for the three shorter alkanols have been offset for clarity. The alkyl chains in the monolayer at the water-hexane interface are progressively disordered from a relatively ordered region near the water to a disordered liquid-like region adjacent to bulk hexane. Hexane is mixed with the monolayer alkyl chain, and water is mixed with the head group region. In the cartoon the long molecules represent the $CH_3(CH_2)_{29}OH$ surfactants, and the short molecules represent hexane (for illustrative purposes only). Figure adapted with permission from Reference 22.

data are analyzed by fitting a model of the electron density profile that consists of two or three slabs, each of constant electron density, sandwiched between bulk water and bulk hexane solution. The slabs are ordered water–1–2–3–hexane. Slab 1 represents the head group region (–CH_2OH), whereas slabs 2 and 3 represent the tail group region [–$(CH_2)_{m-2}CH_3$]. The interface is roughened by capillary waves whose amplitude is determined by the interfacial tension, which is measured separately using the Wilhelmy plate method. Because X-ray reflectivity measures the electron density profile as a function of z, but averaged over the x-y plane, one can model the effect of capillary waves on the reflectivity by a smooth crossover in the electron density from one slab to its neighboring slab or bulk phase. A general formula for the electron density gradient normal to a surface with M slabs is (77)

$$\frac{d\,\langle\rho_e(z)\rangle_{xy}}{dz} = \sum_{i=0}^{M}(\rho_i - \rho_{i+1})\frac{1}{\left(2\pi\sigma_{i+1}^2\right)^{1/2}}\, e^{-(z-D_i)^2/2\sigma_{i+1}^2}, \qquad (3)$$

where ρ_o is the electron density of the water, ρ_{M+1} is the density of the upper oil phase, and the Gaussian functions provide a smooth crossover between slabs i and $i+1$ with an interfacial width σ_{i+1} (the same value of σ_{i+1} is used for all i to model the effect of capillary waves). If L_i is the thickness of the i-th slab, then $D_i = \sum_{j=1}^{i} L_j$ is the distance from the surface of the water to the interface between the i-th and $(i+1)$st slabs.

3. TAIL GROUP EFFECTS

Figure 2*b* illustrates the electron density profiles that yield the best fits to the data shown in **Figure 2*a*** (22). A quantitative analysis of the fitting supports the following conclusions that specify the disordered nature of these *n*-alkanol [$CH_3(CH_2)_{m-1}OH$] monolayers. The average area per alkanol at the water-hexane interface is 23 ± 1 Å^2, larger than the close-packed area of 18.7 Å^2. The tail group is disordered, with progressively more disorder when proceeding from the head group to the terminal methyl group. This conclusion is based on numerical comparison of the electron density profile with values of the electron densities of bulk phases and the molecular ordering in the bulk phases as determined by diffraction or spectroscopy. The ordering in the region of the tail group adjacent to the head group (with an electron density of 0.317 e^- Å^{-3}) is similar to the structure of α (rotator) bulk phases of alkyl chains. Ordering in the rest of the tail group (with an electron density of 0.267 e^- Å^{-3} over more than half the alkyl chain) is similar to the conformation of liquid alkyl chains just above the melting point of bulk alkanes. These experiments place an upper limit on the amount of hexane mixed into the region of the tail group (one hexane for every five or six alkanols). Also, the head group region contains a small fraction of water (approximately one water for every three alkanols). These last two conclusions are based on the number of electrons measured in the slabs that correspond to the interfacial depth of the tail groups and head groups, as well as a consideration of the volume occupied by alkanols.

The disordered nature of these long, flexible alkyl tails is not surprising when the gain in conformational entropy of the tail groups is considered. However, similar

molecular ordering of these alkanols has not been observed at the water-vapor interface. Instead, investigators have observed only solid monolayer phases of close-packed, essentially all-*trans* tail groups at this interface (22–25, 41). The presence of the hexane has produced a large change in the monolayer, but not because of a large fraction of hexane intercalated into the monolayer as proposed by Davies & Rideal (8).

Alternatively, X-ray reflectivity experiments of surfactants with rigid-rod tail groups indicate that the surfactants form close-packed monolayers that fully exclude hexane. Measurements of the interface between hexane solutions of $CF_3(CF_2)_{m-3}(CH_2)_2OH$ (total carbon number $m = 10$ or 12) and water demonstrate the presence of a surfactant monolayer that can be described by a single slab (in this case, the much greater electron density of the fluorinated part of the tail group and the shorter chain renders these reflectivity measurements insensitive to the head group) (12, 13, 38, 57). The electron density $\rho_e = 0.635 \pm 0.01\ e^-\ \text{Å}^{-3}$ that corresponds to the fluorinated part of the tail group of a monolayer of $CF_3(CF_2)_9(CH_2)_2OH$ at the water-hexane interface ($T = 32°C$) lies between the known densities of the monoclinic crystal phase and the rhombohedral rotator solid phase of bulk fluoroalkanes (e.g., for n-$C_{20}F_{42}$) (78). The measured thickness of this slab, 1.25 ± 0.03 nm, corresponds precisely to the calculated length of the fluorinated part of the tail group, which is 1.27 nm. These measurements exclude the possibility that this monolayer could be in a liquid monolayer phase or could have any substantial concentration of hexane.

These measurements suggest that surfactants with rigid-rod tail groups whose shape allows them to pack closely will do so at the water-oil interface, thereby excluding the oil from the interfacial layer, even if the surfactants are soluble in the oil. Conversely, soluble surfactants with flexible tail groups can form loosely packed liquid monolayer phases with disordered tail groups. However, they can also form solid close-packed monolayer phases, as demonstrated below.

4. HEAD GROUP EFFECTS

N-alkanol and *n*-alkanoic acids differ slightly in their chemical composition. When adsorbed to pH 2 water, the alkanoic acid head group is neutral, as is the alkanol head group. Nevertheless, the X-ray reflectivity measurements shown in **Figure 3*a*** from monolayers of $CH_3(CH_2)_{29}OH$ and $CH_3(CH_2)_{28}COOH$ at the water-hexane interface exhibit oscillations of different amplitude (14). The alkanoic acid tail group can be described by a single slab of electron density $0.317 \pm 0.003\ e^-\ \text{Å}^{-3}$ that is comparable with the density in the α-rotator solid phases of long-chain alkanes, in contrast to the alkanol molecules that exhibit liquid-like chain disorder at the interface (79). The $CH_3(CH_2)_{28}COOH$ layer is slightly thicker than the $CH_3(CH_2)_{29}OH$ layer, as indicated by the interference minima appearing at slightly smaller Q_z. The area per molecule of $19 \pm 1\ \text{Å}^2$ determined by the reflectivity measurements is also consistent with a close-packed solid monolayer. We have also measured solid-monolayer ordering for shorter alkanoic acids with 18 and 20 carbons (A.M. Tikhonov & M.L. Schlossman, unpublished data). Analysis of the reflectivity is consistent with the molecular dynamics simulation shown in **Figure 3*b***, including the slight tilt of the molecules.

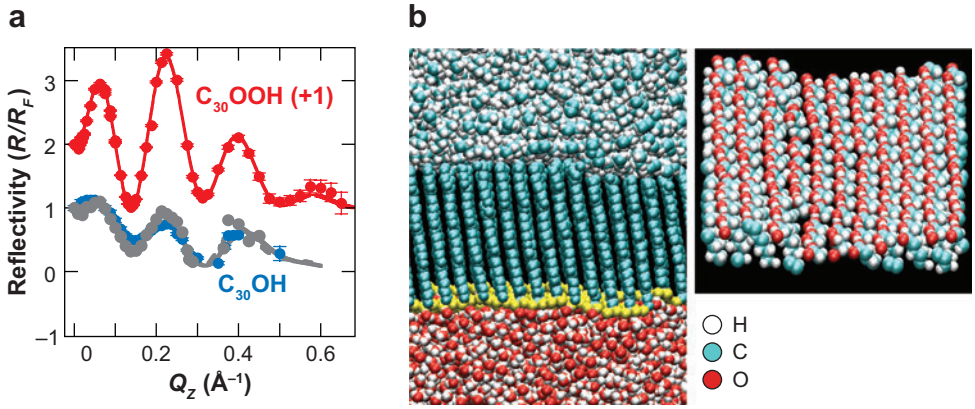

Figure 3

(*a*) Comparison of reflectivity data for triacontanol [$CH_3(CH_2)_{29}OH$, denoted $C_{30}OH$ in figure] and triacontanoic acid [$CH_3(CH_2)_{28}COOH$, denoted $C_{30}OOH$ in figure] monolayers at the water-hexane interface. Chains are disordered for triacontanol monolayers, but ordered for triacontanoic acid monolayers. **Figure 3***a* reprinted with permission from Reference 93. (*b*) Molecular dynamics simulation of a triacontanoic acid monolayer at the water-hexane interface. H atoms are shown in white, C atoms in blue, and O atoms in red, except that head groups of triacontanoic acid in the left panel are shown in yellow. (*Left panel*) The ordered all-*trans* alkyl tails. This side view of the interface shows, from bottom to top, water, triacontanoic acid, and hexane. (*Right panel*) Nearly parallel rows of hydrogen bonds between adjacent –COOH head groups (bottom view of interface) with hexane, water molecules, and most of the surfactant tail removed. The simulation cell size was 54.3 Å × 57.2 Å × 92.0 Å (normal to the interface) and contained 2720 water molecules, 475 hexane molecules, and 136 triacontanoic acid molecules. **Figure 3***b* reprinted with permission from Reference 14.

The molecular dynamics simulation also indicates the presence of hydrogen-bonded head groups arranged in rows (**Figure 3*b***) (14). Because literature values lead to an estimate of approximately five gauche conformations in the disordered portion of the $CH_3(CH_2)_{29}OH$ tail group (22, 80), the attractive energy gained by hydrogen bonding of the alkanoic acid head groups (~5 kcal mol^{-1} per bond) is comparable to the conformational free energy lost (~0.6 kcal mol^{-1} per gauche conformation) when a disordered tail becomes all *trans*. This demonstrates the plausibility of a model in which the presence of the attractive hydrogen bonding brings the alkanoic acid surfactants closer together while ordering what would otherwise be a partially disordered tail group. The chain ordering is more favorable when hydrogen bonds link a row of head groups [as for $CH_3(CH_2)_{28}COOH$], rather than just bonding isolated pairs (or triplets) of head groups [as observed in the molecular dynamics simulation of $CH_3(CH_2)_{29}OH$, not shown] because the ratio of total hydrogen-bonding energy to total conformational free energy is greater. One can also consider the effect of hydrogen bonding on these monolayers in terms of an elastic free energy that describes the stretching of the alkyl tail from the shorter, disordered $CH_3(CH_2)_{29}OH$ to the longer all-*trans* $CH_3(CH_2)_{28}COOH$ (14).

5. PHASE TRANSITIONS AND INHOMOGENEOUS PHASES

Interfacial tension measurements as a function of temperature, bulk pressure, and composition can be used to determine the interfacial phase diagram of water-oil-surfactant systems (15, 35–37). **Figure 4*a*,*b*** presents examples of the tension as a function of temperature $\gamma(T)$. The slope of the tension curve $\gamma(T)$ determines the interfacial excess entropy per unit area, $S_a^\sigma = -(\partial\gamma/\partial T)_{p,c}$, which is the excess entropy of molecules at the interface over their entropy in the bulk (39). The location of the slope discontinuity in the tension curves in **Figure 4** identifies the location of a phase transition whose temperature can be tuned by varying the surfactant concentration and the bulk pressure [although changes in pressure on the order of megapascals

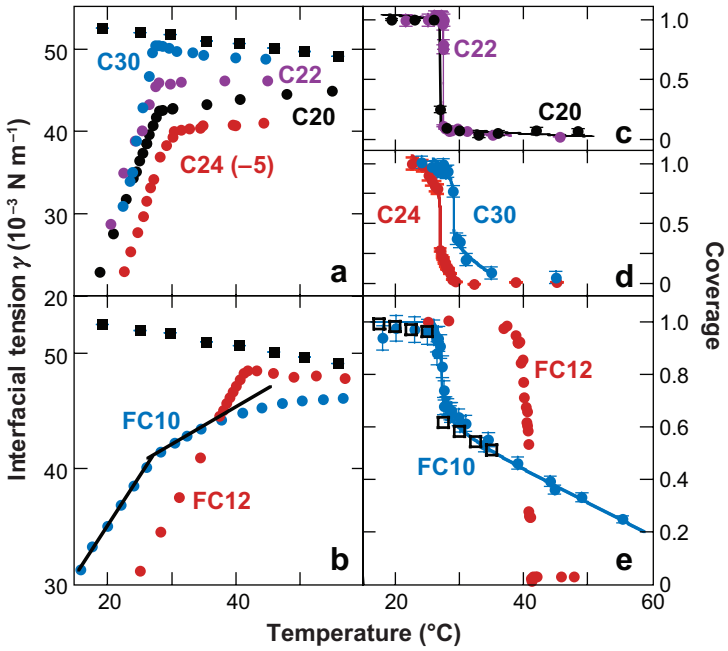

Figure 4

(*a*) Interfacial tension as a function of temperature for hydrocarbon alkanols at the water-hexane interface. C*m* refers to $CH_3(CH_2)_{m-1}OH$. For comparison, the pure water-hexane interface is shown by the black squares. C20 is at 15 mmol kg^{-1} (*black dots*), C22 at 7 mmol kg^{-1} (*purple dots*), C24 at 3 mmol kg^{-1} (*red dots*, displaced down by 5 mN m^{-1} for visual clarity), and C30 at 0.7 mmol kg^{-1} (*blue dots*). (*b*) Interfacial tension as a function of temperature for fluorocarbon alkanols at the water-hexane interface. FC*m* refers to $CF_3(CF_2)_{m-3}(CH_2)_2OH$. Black squares represent the pure water-hexane interface. Lines are provided as a guide to the eye. FC10 is at 5.0 mmol kg^{-1} (*blue dots*) and FC12 at 2.0 mmol kg^{-1} (*red dots*). (*c–e*) Domain coverage (fraction of the interface covered by surfactant domains) as a function of temperature determined from X-ray reflectivity measurements. Labeling similar to panels *a* and *b*. Lines are a theoretical fit (13, 22, 82). Open squares in panel *e* represent the thermodynamic coverage determined from interfacial tension measurements (57).

are required for a noticeable effect (15)]. The close proximity in temperature of the phase transitions in **Figure 4*a*** results from a judicious choice of bulk concentration.

At temperatures below the transition temperature, the large positive slope in $\gamma(T)$ indicates that the entropy of molecules at the interface is much smaller than in the bulk. Above the transition, the excess interfacial entropy is either slightly negative or slightly positive. Therefore, with increasing temperature, the interface undergoes an order-disorder transition. X-ray reflectivity measurements reveal an abrupt reduction in surfactant adsorption at the phase transition. Presumably, surfactants that leave the interface are solvated in the oil phase. The surfactants are vaporized (or sublimated) from the lower-temperature liquid (or solid) monolayer into the dilute oil solution. At high temperatures, the interfacial surfactant density is very low, and the behavior of the interface approaches that of the neat water-hexane interface, for which $\gamma(T)$ has a slightly negative slope. Some interfacial tension measurements suggest that the change in slope from slightly positive to slightly negative [e.g., for $CF_3(CF_2)_7(CH_2)_2OH$, denoted FC10 in **Figure 4*b***] occurs via a second phase transition (19), rather than just a crossover, although structural measurements such as X-ray scattering have not been able to confirm this. However, tension measurements as a function of bulk pressure provide clear evidence for the existence of two phase transitions (17).

As an example, let us consider the phase transition that occurs for monolayers of $CH_3(CH_2)_{m-1}OH$ ($m = 20, 22$) at the water-hexane interface (**Figure 4*a***) (22). In this case, X-ray reflectivity below the transition is essentially unchanged with temperature, except for the effect of interfacial roughness that varies with temperature because the tension is temperature dependent. At the transition, the reflectivity curve changes abruptly (over approximately 0.02°C) to that of an interface without a monolayer. At temperatures above the transition, measurements of an interfacial width larger than that expected from a neat water-hexane interface provide indirect evidence for the existence of a small number of surfactant molecules at the interface, much fewer than in a full monolayer. **Figure 4*c*** illustrates the domain coverage of the interface, which is the fraction of interface covered by surfactant domains. The coverage changes abruptly at the transition from one, which indicates an interface fully covered by the monolayer, to nearly zero. This first-order transition occurs between a condensed liquid monolayer phase and a dilute gaseous monolayer.

Increasing the chain length of $CH_3(CH_2)_{m-1}OH$ to $m = 24$ or 30 or changing the surfactant to $CF_3(CF_2)_{m-3}(CH_2)_2OH$ ($m = 10$ or 12) alters the character of the phase transition (**Figure 4*d*,*e***) (13, 22). The most thoroughly investigated system is $CF_3(CF_2)_9(CH_2)_2OH$, which has been studied with GISAXS and Brewster angle microscopy, as well as X-ray reflectivity (12, 13, 30, 38). The interfacial coverage for $CF_3(CF_2)_9(CH_2)_2OH$ at the water-hexane interface is qualitatively similar to that shown in **Figure 4*c*** for $CH_3(CH_2)_{19}OH$ except that the crossover at the transition is rounded with a width of ~2°C (**Figure 4*e***). GISAXS measurements in **Figure 5*a*** reveal that in the transition region, the interface is in a domain phase that consists of solid monolayer domains separated by dilute gaseous regions (of nearly pure water-hexane interface) (38). The two peaks adjacent to the specular peak represent small-angle scattering from the interfacial domains. Under the assumption that the domains

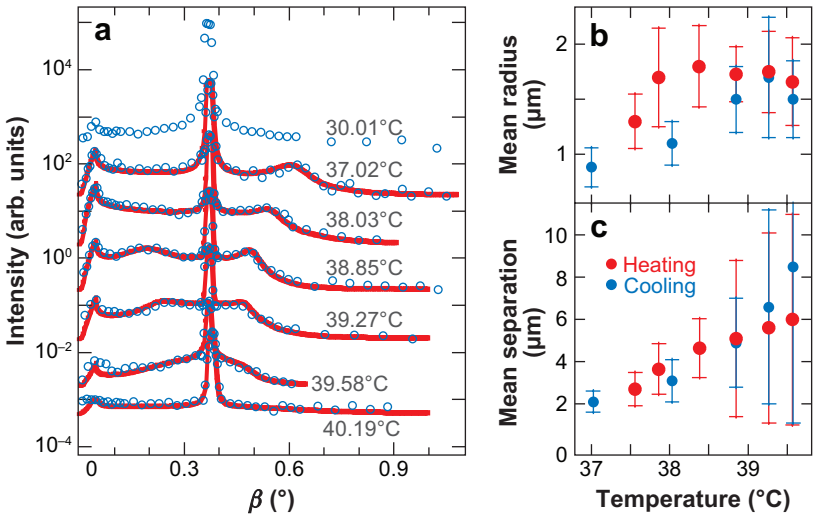

Figure 5

(*a*) Off-specular diffuse scattering (or grazing-incidence small-angle X-ray scattering) from the interface between water and a 2 mmol kg^{-1} solution of $CF_3(CF_2)_9(CH_2)_2OH$ in hexane measured on cooling through the phase transition. Curves displaced for clarity. Similar data (not shown) are measured on heating through the transition. The transition temperature is between the two highest temperatures (i.e., 39.58°C and 40.19°C). Above the transition, the interface is nearly free of surfactants. Surfactant domains are present below the transition. The tall peaks at $\beta = 0.37°$ at all temperatures are the specular reflectivity. The small peaks at $\beta = 0.045°$ result from a surface field enhancement effect that indicates the presence of interfacial inhomogeneities. Additional scattering and peaks above the background (as observed at 40.19°C) represent small-angle scattering from interfacial domains. (*b*) Mean radius of domains, assumed to be circular, and (*c*) mean separation between domain centers determined from off-specular diffuse scattering data taken while heating (*red*) and cooling (*blue*) through the transition. The vertical lines in panels *b* and *c* illustrate the polydispersity in radius and separation. Figure adapted with permission from Reference 38.

are circular, further analysis reveals that the average domain radius is ∼1.5 μm (**Figure 5*b***), and the average domain separation varies from 2 μm at the lowest temperatures (when the radius is 1 μm and the domains fill the interface) to ∼8 μm close to the transition (**Figure 5*c***). The domain phase near the transition is reproducible on heating or cooling through the transition, without any measurable hysteresis.

The constancy of the domain size under conditions at which the interfacial concentration of surfactants changes by a factor of 20 indicates that domains are created or annihilated on cooling or heating. Thus, the surfactants at the interface can exchange with those in the bulk to allow full equilibration of these systems. Above the transition region, all evidence of domains disappears. Brewster angle microscope images provided further evidence for domains in this system, although the domain size was below the optical resolution (∼10 μm) of the microscope (30).

In a slightly shorter fluorinated surfactant, $CF_3(CF_2)_7(CH_2)_2OH$, the domain phase persists over a much larger range of temperature. **Figure 4*e*** shows that

although the coverage changes abruptly at the transition, it changes by only ∼30%. Above the transition the coverage further decreases gradually over tens of degrees Celsius. All the X-ray reflectivity curves throughout this temperature range exhibit the same interference pattern, differing only in the amplitude of the interference fringe (57). Therefore, the thickness of the monolayer is unchanged, but its average electron density changes with temperature. The coverage shown in **Figure 4*e*** is produced by assuming that the domains have the same molecular ordering as the low-temperature phase that fully covers the interface. **Figure 4*e*** also demonstrates that the domain coverage produced by this analysis agrees with values of the thermodynamic coverage derived from interfacial tension measurements as a function of both surfactant concentration and temperature (57).

Arguably, the reflectivity data may be equally well explained by a homogeneously covered interface in which the $CF_3(CF_2)_7(CH_2)_2OH$ molecules are progressively displaced from their neighbors with increasing temperature. Although one could object to this model on purely physical grounds, the X-ray reflectivity provides further justification for the presence of domains. The analysis of reflectivity from inhomogeneous phases requires consideration of the X-ray coherence, that is, whether X rays reflected from different positions on the interface will add coherently or incoherently. The results for the coverage, above the phase transition, differ by more than a factor of two when analyzed using coherent or incoherent reflections (13). Agreement with the thermodynamic coverage occurs only for coherent reflections, suggesting that the domain size is smaller than the ∼5 μm coherence length (22). This is consistent with the domain size measured for the slightly longer $CF_3(CF_2)_9(CH_2)_2OH$ (30). Similar considerations have also been documented for the hydrocarbon surfactants $CH_3(CH_2)_{m-1}OH$ ($m = 24, 30$) that exhibit rounding of the coverage near the transition (**Figure 4*c***) (22).

The Gibbs phase rule indicates that these interfaces with domains are not coexistent regions of two interfacial phases, but rather are a single inhomogeneous phase. As shown elsewhere, this is a consequence of our observations that the domains are observed over a range of temperatures, that the domains are in equilibrium, and that the role of impurities seems to be negligible (22). The thermodynamic variance w of this system is given by $w = 2+(c-r)-\phi-(\psi-s)$, where $c = 3$ is the number of components (water, hexane, and surfactant), $r = 0$ is the number of chemical reactions, $\phi = 2$ is the number of bulk phases, $s = 1$ is the number of types of interfaces, and ψ is the number of interface phases (81). This expression for the variance is appropriate for systems in which the interface phases are contiguous (so only the liquid-liquid interface is considered) and the interface is flat.

For one interfacial phase ($\psi = 1$, $w = 3$), we can determine the state of the interface by specifying three intensive thermodynamic variables, such as temperature, bulk pressure, and surfactant concentration. If there are two interfacial phases ($\psi = 2$, $w = 2$), then they can coexist at only one temperature for a given bulk pressure and alkanol concentration. If the presence of domains indicates a coexistence between two phases, then that coexistence can occur at only one temperature. However, domains are observed over a range of temperatures for a given bulk pressure and concentration. An alternative explanation is that the interface is in a single spatially inhomogeneous

phase. In this case, the interfacial concentration of surfactants is not isotropic, but varies within the interface owing to the presence of domains. As discussed elsewhere, it is unlikely that the presence of impurities or nonequilibrium effects could invalidate this application of the phase rule (22).

Researchers have shown theoretically that spatially inhomogeneous phases result from competing interactions in both two- and three-dimensional systems (82, 83). In the case of monolayers of polar molecules, the van der Waals forces act as a short-range-attractive interaction, and the dipoles of the surfactants produce a long-range-repulsive interaction. Extensive theoretical work in a variety of areas of condensed matter has demonstrated that such competing interactions can stabilize single phases whose order parameter (i.e., the interfacial density in the case of surfactant monolayers) varies spatially throughout the phase. Andelman and coworkers (83) introduced the idea that a sufficiently strong repulsive interaction produces inhomogeneous phases of organic monolayers in the region of the phase diagram that would otherwise be occupied by the liquid-gas critical point. Archer & Wilding (84) recently suggested a phase diagram for three-dimensional systems as a function of chemical potential μ, the inverse of the amplitude of attractive interactions ε^{-1}, and the amplitude of the repulsive interactions. **Figure 6** shows a cut through this phase diagram for a fixed amplitude of repulsive interactions.

Application of the theoretical development of inhomogeneous phases to our experimental results is not without difficulties. Our earliest application involved a scaling theory of a critical phase transition developed by Marchenko (82) for magnetic

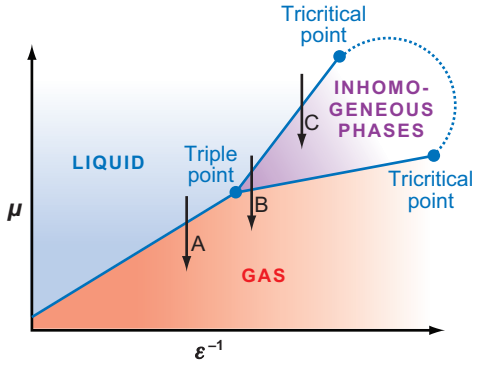

Figure 6

Phase diagram suggested by Archer & Wilding (84) for three-dimensional inhomogeneous phases. The chemical potential μ is shown as a function of the inverse of the amplitude of attractive interactions ε^{-1} for a large, fixed amplitude of repulsive interactions. For a small repulsive interaction, the region shown would contain the liquid-gas critical point and only homogeneous phases. For a large repulsive interaction, the critical point is replaced by the phase behavior illustrated in the figure. Transitions can occur between the homogeneous liquid or gas phase and inhomogeneous phases. Also, transitions between inhomogeneous phases are predicted to occur in the region labeled "inhomogeneous phases." Paths A, B, and C may represent experiments on an alkanol monolayer at the water-hexane interface in which the temperature is varied. Figure adapted with permission from Reference 84.

systems. We can rewrite Marchenko's prediction for the interfacial polarization in terms of domain coverage of a surfactant system as

$$C(T) - C(T_c) = b\ sign(T_c - T)[\ln(T_c/|T_c - T|)]^{-a} \quad \text{for} \quad T \to T_c, \qquad (4)$$

where T_c is the phase-transition temperature, $C(T_c)$ is the domain coverage at the transition, and a and b are positive constants related to scaling parameters in the theory (13, 22). The theory cannot predict the constants a and b, so we investigated the variation of these parameters obtained by fitting our data (the lines in **Figure 4*c*,*d*,*e*** are fits to Equation 4). Although the functional form in Equation 4 allows the data to be fit, the six systems we have studied did not produce an understanding of the variation of these parameters with the system (22). Also, the Marchenko theory describes a critical transition, whereas the X-ray data, particularly for $CH_3(CH_2)_{19}OH$ and $CH_3(CH_2)_{21}OH$, indicate that the transition is first order (**Figure 4*c***).

Further insight may be provided by comparing our data with the phase diagram in **Figure 6**. Although **Figure 6** was suggested for three-dimensional systems, we use it as a guide to the behavior of a monolayer. The surfactant chemical potential of the dilute oil solution is $\mu = \mu^\circ + RT \ln c$, where c is the bulk concentration. Therefore, increasing the temperature is equivalent to lowering the chemical potential. As discussed above, the coverage curve for FC12 [$CF_3(CF_2)_9(CH_2)_2OH$] shown in **Figure 4*e*** indicates a transition from a condensed low-temperature monolayer phase through a region of an inhomogeneous phase that covers a small range in temperature (~2°C) to a region of a gas phase. This may be equivalent to path B indicated in **Figure 6**. The slightly shorter surfactant FC10 [$CF_3(CF_2)_7(CH_2)_2OH$; see **Figure 4*e***] undergoes a transition from a condensed monolayer phase at low temperatures to an inhomogeneous phase that persists over tens of degrees Celsius. Because FC10 is shorter than FC12, but otherwise similar in composition, the attractive van der Waals forces are smaller, and the appropriate path through the phase diagram should be at larger ε^{-1}. These results are consistent with path C indicated in **Figure 6**. Although these results are suggestive, a difficulty persists. The low-temperature phases measured for FC10 and FC12 are solid phases, not liquid as discussed by the theory. Whether this theory will apply to these pseudo-two-dimensional solid phases that may not exhibit long-range positional order is unclear. Also unclear is the exact nature of the spatial and orientational correlations in these systems.

The application of the theory in **Figure 6** to the case of $CH_3(CH_2)_{m-1}OH$ surfactants, which exhibit a liquid monolayer phase, is problematic. As illustrated in **Figure 4*c***, C20 and C22 [$CH_3(CH_2)_{19}OH$ and $CH_3(CH_2)_{21}OH$] undergo a first-order phase transition from a liquid to gas monolayer, similar to path A in **Figure 6**. Because we expect the longer alkanols C24 and C30 [$CH_3(CH_2)_{23}OH$ and $CH_3(CH_2)_{29}OH$] to have greater van der Waals attraction, the path through the phase diagram should be at smaller ε^{-1}, that is, a path to the left of path A in **Figure 6**. This would indicate that longer alkanols should also just exhibit a simple liquid-gas transition. However, the temperature variation of the coverage for C24 and C30 (**Figure 4*d***) indicates partial coverage of the interface for a few degrees both above and below an abrupt change in coverage. It is not clear whether this sequence of coverage results from pretransition effects on either side of the transition

or if it represents a monolayer phase sequence of (*a*) homogeneous liquid to inhomogeneous phase I, (*b*) inhomogeneous phase I to inhomogeneous phase II, and (*c*) inhomogeneous phase II to homogeneous gas. If interpreted as three transitions, then the coverage changes continuously at transitions (*a*) and (*c*), but abruptly at (*b*). Of equal importance, the variation of interfacial tension with temperature exhibits one kink, which indicates a first-order phase transition [e.g., transition (*b*)], although smaller changes in the slope within a few degrees of this transition may indicate the presence of transitions (*a*) and (*c*). It is possible that accounting for the conformational degrees of freedom of these molecules will allow for agreement between theory and experiment; however, the phase sequence of the hydrocarbon alkanols is still an open issue.

6. SOLVENT EFFECTS ON ORDERING AND MULTILAYERING TRANSITIONS

Two important features of surfactant ordering at the water-alkane interface depend on the relative chain lengths of the alkane solvent and the surfactant (26). First, there is a strong dependence of the structure of the adsorbed layer on the length of the alkane used for the solvent. Second, the nature of the adsorption, or vaporization, transition changes dramatically when the alkanol chain is only six to eight carbons longer than the solvent alkane chain.

To characterize these features, we used interfacial tension data to calculate ΔS_a^σ, which is the change in interfacial excess entropy per unit area at the phase transition (i.e., the transition indicated by the kink in curves similar to those shown in **Figure 4*a***). **Figure 7** illustrates ΔS_a^σ versus r, where $r = m/m_o$ is the ratio of the alkanol surfactant carbon number m to the alkane solvent carbon number m_o, and ΔS_a^σ was determined from tension measurements of a water interface with either a

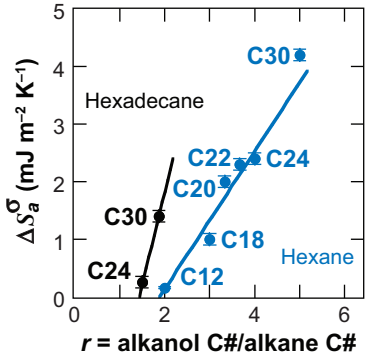

Figure 7

Change in interfacial excess entropy per unit area across the transition ΔS_a^σ versus r for solutions in hexane (*blue*) and in hexadecane (*black*), where $r = m/m_o$ is the ratio of the alkanol carbon number m to the alkane solvent carbon number m_o. Symbols are labeled with Cm, which refers to $CH_3(CH_2)_{m-1}OH$. Figure adapted with permission from Reference 26.

hexane solution or a hexadecane solution of hydrocarbon alkanols (26). For a given solvent, ΔS_a^σ approaches zero as the chain length of the surfactant is reduced to within approximately six carbons of the solvent chain length. Consistent with this, for a given alkanol chain length, the value of ΔS_a^σ is smaller at the water-hexadecane than at the water-hexane interface.

The difference in ΔS_a^σ for $CH_3(CH_2)_{29}OH$ at the two interfaces indicates that $CH_3(CH_2)_{29}OH$ is less ordered in the low-temperature interfacial phase at the water-hexadecane interface than at the water-hexane interface because there is only a small difference in the interfacial excess entropies above the transition. Indeed, the X-ray reflectivity measurements reveal a large difference in the ordering of $CH_3(CH_2)_{29}OH$ monolayers in the low-temperature phase (26). At the water-hexane interface (as discussed above), the portion of the tail group near the head group is ordered like a rotator alkane phase, but it becomes progressively more disordered further from the head group until the ordering is liquid-like in the half of the chain that includes the terminal methyl group. At the water-hexadecane interface, reflectivity measurements indicate that the entire tail group of $CH_3(CH_2)_{29}OH$ is disordered.

A more striking effect is produced when ΔS_a^σ approaches zero. **Figure 8*a*** illustrates the difference between the reflectivity for $CH_3(CH_2)_{23}OH$ at the water-hexane ($\Delta S_a^\sigma = 2.4 \pm 0.1$ mJ m^{-2} K^{-1}) and water-hexadecane ($\Delta S_a^\sigma = 0.26 \pm 0.05$ mJ m^{-2} K^{-1}) interfaces, and **Figure 8*b*** displays the electron density profiles for these interfaces (26). The unusual form of the reflectivity from $CH_3(CH_2)_{23}OH$ at

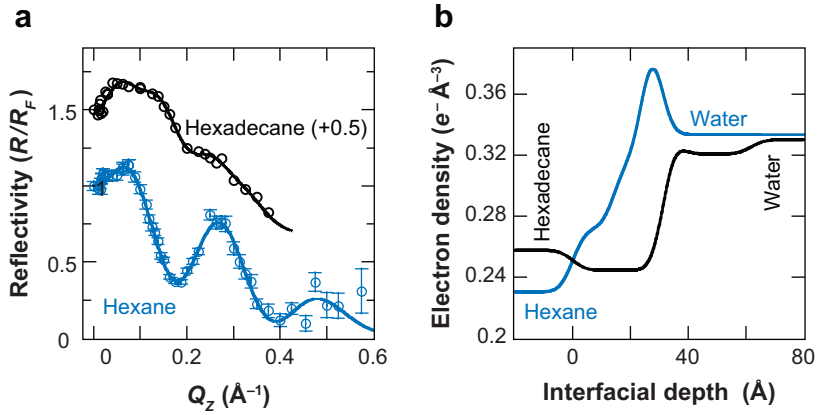

Figure 8

Studies of the interface between water and a hexane or hexadecane solution of $CH_3(CH_2)_{23}OH$ at temperatures well below the phase transition. (*a*) X-ray reflectivity (normalized to the Fresnel reflectivity) as a function of the wave-vector transfer from $CH_3(CH_2)_{23}OH$ in the low-temperature phase at the water-hexane ($T = 21.9$°C, *blue*) and water-hexadecane ($T = 50.8$°C, *black*) interfaces. The solid blue line represents a three-slab model of a monolayer, and the solid black line represents a two-slab model of a bilayer. (*b*) Electron density profiles determined from the fits in panel *a*. $z = 0$ is bulk hexane (*blue*) or hexadecane (*black*). $CH_3(CH_2)_{23}OH$ forms a monolayer at the water-hexane interface and a bilayer at the water-hexadecane interface. Figure reprinted with permission from Reference 26.

the water-hexadecane interface cannot be fit with a monolayer. Instead, a bimolecular layer is formed at the water-hexadecane interface (**Figure 8*b***). The average electron density of the first layer (0.323 e^- Å^{-3}) corresponds to a rotator solid phase, but the electron density of the second layer is much smaller (0.247 e^- Å^{-3}), indicating that this layer is disordered. The second layer is possibly only a partial layer, but these measurements cannot determine that. Similarly, the other system that we measured with a very low ΔS_a^σ (0.16 ± 0.02 mJ m^{-2} K^{-1}), $CH_3(CH_2)_{11}OH$ at the water-hexane interface, exhibits interfacial multilayering of three or four molecular layers. In this case, the layers are also progressively more disordered starting from the layer closest to water. These results suggest that a layer-by-layer wetting transition is approached as ΔS_a^σ approaches zero (26).

7. CONCLUSIONS

The recent application of X-ray surface scattering to study the molecular ordering and phase behavior of surfactants at the interface between water and an oil solution of surfactants has led to a greatly revised understanding of these important interfacial structures. X-ray reflectivity provides information on the molecular ordering of the surfactants with subnanometer spatial resolution as a function of depth into the interface. Off-specular diffuse scattering probes the in-plane structure of inhomogeneous phases. Together, these techniques have demonstrated that neither studies of Langmuir monolayers of surfactants at the water-vapor interface nor the traditional view of liquid-liquid interfaces espoused by Davies & Rideal (8) provides a good guide to these interfaces.

The studies presented here have begun to address a number of fundamental issues of surfactant ordering at the water-oil interface. The role of tail group flexibility on surfactant ordering was studied by examining fluorocarbon alkanols with rigid rod tails and hydrocarbon alkanols with flexible tails. The result that the fluorocarbon alkanols formed ordered solid phases and the hydrocarbon alkanols formed disordered liquid phases was not surprising, except possibly in light of corresponding experiments at the water-vapor interface in which both types of molecules form solid phases. The importance of complex interactions was revealed by the study of hydrocarbon alkanoic acids, which formed an ordered solid phase at the water-hexane interface. This phase was most likely driven to its ordered state by hydrogen bonding between the acid head groups whose attractive interaction overcame the disordering effect of the long flexible tail groups.

Variation of the oil solvent can also affect surfactant ordering, as demonstrated by many studies of interfacial tension (e.g., see 37, 85). Evidence from computer simulations, theoretical modeling, and interfacial tension measurements indicates that steric matching of the solvent chain length with some aspect of the surfactant architecture can alter the interfacial ordering (86–88). Here, we demonstrated that increasing the length of the alkane solvent molecules to be closer to, but not matching, the length of the alkanol surfactants leads to a markedly different ordering of the interfacial molecules. As a critical chain-length difference of approximately six carbons is approached, the interfacial monolayer is converted to a multilayer.

In addition to this observation of surfactant multilayers at the water-oil interface, a number of other observations indicate the importance of multilayer or thicker structures at the water-oil interface. For example, the multilayering of lipids at the water-alkane interface produces macroscopically thick layers and vesicle budding (89; for a review on the formation of thick films of amphiphiles at liquid-liquid interfaces, see Reference 90, and references therein). A 60-Å-thick multilayer of hexadecylphosphorylcholine at the water-hexadecane interface has been measured recently by neutron reflectivity (91). Moreover, macroscopically thick layers are formed at the interface between crude oil and water, the so-called rag layer (92).

Surfactants at water-oil interfaces exhibit a rich phase structure consisting of homogeneous and inhomogeneous phases comprising liquid, solid, and gas monolayer regions. X-ray studies have probed these transitions as a function of temperature, which allows for variation of the surfactant chemical potential. A satisfactory correspondence between these experimental results and theory does not exist. It might be expected that such spatially inhomogeneous phases could also exist at the internal surfactant interfaces in water-in-oil or oil-in-water emulsions, as well as at other internal interfaces, but we are not aware of such observations.

Although these X-ray measurements carried out during the past decade have revealed new features of surfactant ordering at the water-oil interface, much remains to be understood. This includes understanding the complex interactions that determine the molecular ordering and phase behavior of the interface, as well as extending these studies to other types of surfactants, such as ionic surfactants and surfactants of a variety of architectures that raise interesting scientific questions and are important for many industrial applications.

DISCLOSURE STATEMENT

The authors are not aware of any biases that might be perceived as affecting the objectivity of this review.

ACKNOWLEDGMENTS

We would like to acknowledge our collaborators on the work discussed above, including Ming Li, Dragoslav Mitrinovic, Sai Venkatesh Pingali, Scott Williams, Zhongjian Zhang, Harshit Patel, and Shekhar Garde. This work was supported by the NSF (DMR-9700975 and DMR-0092469). Beamline X19C has received support from the NSF (CHE-9200080), the University of Chicago, and the University of Illinois at Chicago. Use of the National Synchrotron Light Source, Brookhaven National Laboratory, was supported by the U.S. Department of Energy, Office of Basic Energy Sciences, under Contract No. DE-AC02–98CH10886.

LITERATURE CITED

1. Als-Nielsen J, McMorrow D. 2001. *Elements of Modern X-Ray Physics*. Hoboken, NJ: Wiley & Sons

2. Daillant J, Alba M. 2000. High-resolution X-ray scattering measurements. I. Surfaces. *Rep. Prog. Phys.* 63:1725–77
3. Kaganer VM, Mohwald H, Dutta P. 1999. Structure and phase transitions in Langmuir monolayers. *Rev. Mod. Phys.* 71:779–819
4. Thomas RK. 2004. Neutron reflection from liquid interfaces. *Annu. Rev. Phys. Chem.* 55:391–426
5. Schlossman ML. 2002. Liquid-liquid interfaces: studied by X-ray and neutron scattering. *Curr. Opin. Colloid Interface Sci.* 7:235–43
6. Richmond GL. 2001. Structure and bonding of molecules at aqueous surfaces. *Annu. Rev. Phys. Chem.* 52:357–89
7. Gelbart WM, Ben-Shaul A, Roux D, eds. 1994. *Micelles, Membranes, Microemulsions, and Monolayers*. New York: Springer-Verlag
8. Davies JT, Rideal EK. 1963. *Interfacial Phenomena*. New York: Academic
9. Davies JT. 1951. The distribution of ions under a charged monolayer, and a surface equation of state for charged films. *Proc. R. Soc. Lond. Ser. A* 208:224–47
10. Taylor JAG, Mingins J, Pethica BA. 1976. Phospholipid monolayers at the *n*-heptane/water interface. Part 2. Dilute monolayers of saturated 1,2-diacyl-lecithins and -cephalins. *J. Chem. Soc. Faraday I* 72:2694–702
11. Yue BY, Jackson CM, Taylor JAG, Mingins J, Pethica BA. 1976. Phospholipid monolayers at non-polar oil/water interfaces. Part 1. Phase transitions in distearoly-lecithin films at the *n*-heptane aqueous sodium chloride interface. *J. Chem. Soc. Faraday I* 72:2685–93
12. Zhang Z, Mitrinovic DM, Williams SM, Huang Z, Schlossman ML. 1999. X-ray scattering from monolayers of $F(CF_2)_{10}(CH_2)_2OH$ at the water-(hexane solution) and water-vapor interfaces. *J. Chem. Phys.* 110:7421–32
13. Tikhonov AM, Li M, Mitrinovic DM, Schlossman ML. 2001. Phase transition behavior of fluorinated monolayers at the water-hexane interface. *J. Phys. Chem. B* 105:8065–68
14. Tikhonov AM, Patel H, Garde S, Schlossman ML. 2006. Tail ordering due to head hydrogen bonding interaction in surfactant monolayers at the water-oil interface. *J. Phys. Chem. B* 110:19093–96
15. Matubayasi N, Motomura K, Aratono M, Matuura R. 1978. Thermodynamic study on the adsorption of 1-octadecanol at hexane/water interface. *Bull. Chem. Soc. Jpn.* 51:2800–3
16. Hayami Y, Uemura A, Ikeda N, Aratono M, Motomura K. 1995. Phase transition of the adsorbed film of 1,1,2,2-tetrahydroperfluorododecanol at the hexane/water interface. *J. Colloid Interface Sci.* 172:142–46
17. Takiue T, Yanata A, Ikeda N, Hayami Y, Motomura K, Aratono M. 1996. Thermodynamic study on phase transition in adsorbed film of fluoroalkanol at the hexane/water interface. 2. Pressure effect on the adsorption of 1,1,2,2-tetrahydrohenicosafluorododecanol. *J. Phys. Chem.* 100:20122–25
18. Takiue T, Yanata A, Ikeda N, Motomura K, Aratono M. 1996. Thermodynamic study on phase transition in adsorbed film of fluoroalkanol at the hexane/water interface. 1. Pressure effect on the adsorption of 1,1,2,2-tetrahydroheptadecafluorodecanol. *J. Phys. Chem.* 100:13743–46

19. Takiue T, Uemura A, Ikeda N, Motomura K, Aratono M. 1998. Thermodynamic study on phase transition in adsorbed film of fluoroalkanol at the hexane/water interface. 3. Temperature effect on the adsorption of 1,1,2,2-tetrahydroheptadecafluorodecanol. *J. Phys. Chem. B* 102:3724–29
20. Takiue T, Matsuo T, Ikeda N, Motomura K, Aratono M. 1998. Thermodynamic study on phase transition in adsorbed film of fluoroalkanol at the hexane/water interface. 4. Phase transition in the adsorbed film of the alkanol and fluoroalkanol mixture. *J. Phys. Chem. B* 102:4906–11
21. Tikhonov AM, Schlossman ML. 2003. Surfactant and water ordering in tricontanol monolayer at water-hexane interface. *J. Phys. Chem. B* 107:3344–47
22. Tikhonov AM, Pingali SV, Schlossman ML. 2004. Monolayer structure and molecular ordering in alkanol monolayers at the water-hexane interface. *J. Chem. Phys.* 120:11822–38
23. Barton SW, Thomas BN, Flom EB, Rice SA, Lin B, et al. 1988. X-ray diffraction study of a Langmuir monolayer of $C_{21}H_{43}OH$. *J. Chem. Phys.* 89:2257–70
24. Lin B. 1990. *X-ray diffraction studies of fatty acid and alcohol monolayers on the surface of water*. PhD thesis. Northwestern Univ., Evanston, Ill.
25. Shih MC, Bohanon TM, Mikrut JM, Zschack P, Dutta P. 1992. X-ray diffraction study of heneicosanol monolayers on the surface of water. *J. Chem. Phys.* 97:4485–88
26. Tikhonov AM, Schlossman ML. 2007. Vaporization and layering of alkanols at the oil/water interface. *J. Phys. Condens. Matter* 19:375101–16
27. Mohwald H. 1988. Direct characterization of monolayers at the air-water interface. *Thin Solid Films* 159:1–15
28. McConnell HM. 1991. Structures and transitions in lipid monolayers at the air-water interface. *Annu. Rev. Phys. Chem.* 42:171–95
29. Seul M, Andelman D. 1995. Domain shapes and patterns: the phenomenology of modulated phases. *Science* 267:476–83
30. Uredat S, Findenegg GH. 1999. Domain formation in Gibbs monolayers at oil/water interfaces studied by Brewster angle microscopy. *Langmuir* 15:1108–14
31. McConnell HM, DeKoker R. 1996. Equilibrium thermodynamics of lipid monolayer domains. *Langmuir* 12:4897–904
32. Schwartz DK, Schlossman ML, Pershan PS. 1992. Re-entrant appearance of phases in a relaxed Langmuir monolayer of tetracosanoic acid as determined by X-ray scattering. *J. Chem. Phys.* 96:2356–70
33. Bommarito GM, Foster WJ, Pershan PS, Schlossman ML. 1996. A determination of the phase diagram of relaxed Langmuir monolayers of Behenic acid. *J. Chem. Phys.* 105:5265–84
34. Buontempo JT, Rice SA, Karaborni S, Siepmann JI. 1993. Differences in the structures of relaxed and unrelaxed Langmuir monolayers of heneicosanol: dependence of collective molecular tilt on chain conformation. *Langmuir* 9:1604–7
35. Motomura K, Matubayasi N, Aratono M, Matuura R. 1978. Thermodynamic studies of adsorption at interfaces II. One surface-active component system: tetradecanol at the hexane/water interface. *J. Colloid Interface Sci.* 64:356–61

36. Lin M, Firpo J-L, Mansoura P, Baret JF. 1979. A phase transition of the adsorbed layer: high pressure effect on fatty alcohol adsorption at an oil-water interface. *J. Chem. Phys.* 71:2202–6
37. Ikenaga T, Matubayasi N, Aratono M, Motomura K, Matuura R. 1980. Solvent effect on the adsorption of 1-octadecanol at oil/water interface. *Bull. Chem. Soc. Jpn.* 53:653–57
38. Li M, Tikhonov A, Schlossman ML. 2002. An X-ray diffuse scattering study of domains in $F(FC_2)_{10}(CH_2)_2OH$ monolayers at the hexane-water interface. *Europhys. Lett.* 58:80–86
39. Lyklema J. 2000. *Fundamentals of Interface and Colloid Science III: Liquid-Fluid Interfaces*. San Diego: Academic
40. Jacquemain D, Leveiller F, Weinbach S, Lahav M, Leiserowitz L, et al. 1991. Crystal structures of self-aggregates of insoluble aliphatic amphiphilic molecules at the air-water interface: an X-ray synchrotron study. *J. Am. Chem. Soc.* 113:7684–91
41. Wang J-L, Leveiller F, Jacquemain D, Kjaer K, Als-Nielsen J, et al. 1994. Two-dimensional structures of crystallin self-aggregates of amphiphilic alcohols at the air-water interface as studied by grazing incidence synchroton X-ray diffraction and lattice energy calculations. *J. Am. Chem. Soc.* 116:1192–204
42. Miranda PB, Du Q, Shen YR. 1998. Interaction of water with a fatty acid Langmuir film. *Chem. Phys. Lett.* 286:1–8
43. Wolfrum K, Laubereau A. 1994. Vibrational sum-frequency spectroscopy of an adsorbed monolayer of hexadecanol on water: destructive interference of adjacent lines. *Chem. Phys. Lett.* 228:83–88
44. Buontempo JT, Rice SA. 1993. Infrared external reflection spectroscopic studies of phase transitions in Langmuir monolayers of heneicosanol. *J. Chem. Phys.* 98:5835–46
45. Buontempo JT, Rice SA. 1993. Infrared external reflection spectroscopic studies of phase transitions in Langmuir monolayers of stearyl alcohol. *J. Chem. Phys.* 99:7030–37
46. Pershan PS. 1990. Structure of surfaces and interfaces as studied using synchrotron radiation: liquid surfaces. *Faraday Discuss. Chem. Soc.* 89:231–34
47. Sinha SK, Sirota EB, Garoff S, Stanley HB. 1988. X-ray and neutron scattering from rough surfaces. *Phys. Rev. B* 38:2297–311
48. Mitrinovic DM, Tikhonov AM, Li M, Huang Z, Schlossman ML. 2000. Noncapillary-wave structure at the water-alkane interface. *Phys. Rev. Lett.* 85:582–85
49. Tikhonov AM, Mitrinovic DM, Li M, Huang Z, Schlossman ML. 2000. An X-ray reflectivity study of water-docosane interface. *J. Phys. Chem. B* 104:6336–39
50. Luo G, Malkova S, Pingali SV, Schultz DG, Lin B, et al. 2005. The width of the water/2-heptanone liquid-liquid interface. *Electrochem. Commun.* 7:627–30
51. Luo G, Malkova S, Pingali SV, Schultz DG, Lin B, et al. 2006. Structure of the interface between two polar liquids: nitrobenzene and water. *J. Phys. Chem. B* 110:4527–30

52. Heilmann RK, Fukuto M, Pershan PS. 2001. Quenching of capillary waves in composite wetting films from a binary vapor: an X-ray reflectivity study. *Phys. Rev. B* 63:205405
53. Li M, Tikhonov AM, Chaiko D, Schlossman ML. 2001. Coupled capillary wave fluctuations in thin aqueous films on an aqueous subphase. *Phys. Rev. Lett.* 86:5934–37
54. Li M, Chaiko D, Schlossman ML. 2003. X-ray reflectivity study of a monolayer of ferritin proteins at a nanofilm aqueous-aqueous interface. *J. Phys. Chem. B* 107:9079–85
55. Fukuto M, Gang O, Alvine KJ, Pershan PS. 2006. Capillary wave fluctuations and intrinsic widths of coupled fluid/fluid interfaces: an X-ray scattering study of a wetting film on bulk liquid. *Phys. Rev. E* 74:031607
56. Paulus M, Gutt C, Tolan M. 2005. Surface roughness and adsorption isotherms of molecularly thin liquid films: an X-ray reflectivity study. *Phys. Rev. E* 72:061601
57. Pingali SV, Takiue T, Luo G, Tikhonov AM, Ikeda N, et al. 2005. X-ray reflectivity and interfacial tension study of the structure and phase behavior of the interface between water and mixed surfactant solutions of $CH_3(CH_2)_{19}OH$ and $CF_3(CF_2)_7(CH_2)_2OH$ in hexane. *J. Phys. Chem. B* 109:1210–25
58. Fradin C, Luzet D, Braslau A, Alba M, Muller F, et al. 1998. X-ray study of the fluctuations and the interfacial structure of a phospholipid monolayer at an alkane-water interface. *Langmuir* 14:7327–30
59. Saint Martin E, Konovalov O, Daillant J. 2007. Studies of phospholipid monolayer at liquid/liquid interface in presence of an antimicrobial peptide. *Thin Solid Films* 515:5687–90
60. Schlossman ML, Mitrinovic DM, Zhang Z, Li M, Huang Z. 1999. X-ray scattering from single liquid-liquid interfaces. *Synchrotron Radiat. News* 12:53–58
61. McClain BR, Lee DD, Carvalho BL, Mochrie SGJ, Chen SH, Litster JD. 1994. X-ray reflectivity study of an oil-water interface in equilibrium with a middle-phase microemulsion. *Phys. Rev. Lett.* 72:246–49
62. Lee DD, McClain BR, Carvalho BL, Mochrie SGJ, Litster JD, et al. 1996. Interfacial scattering from surfactant monolayers in microemulsions. *Phys. B* 221:296–300
63. Mitrinovic DM, Williams SM, Schlossman ML. 2001. X-ray study of oil-microemulsion and oil-water interfaces in ternary amphiphilic systems. *Phys. Rev. E* 63:021601
64. McClain BR, Yoon M, Litster JD, Mochrie SGJ. 1999. Interfacial roughness in a near-critical binary fluid mixture: X-ray reflectivity and near-specular diffuse scattering. *Eur. Phys. J. B* 10:45–52
65. Lin Y, Skaff H, Emrick T, Dinsmore AD, Russell TP. 2003. Nanoparticle assembly and transport at liquid-liquid interfaces. *Science* 299:226–29
66. Tikhonov AM. 2006. X-ray study of the electric double layer at the *n*-hexane/nanocolloidal silica interface. *J. Chem. Phys.* 124:164704
67. Tikhonov AM. 2006. Water density in the electric double layer at the insulator/electrolyte solution interface. *J. Phys. Chem. B* 110:2746–50
68. Tikhonov AM. 2007. Wigner crystals of Na^+ at the surface of a silica hydrosol. *J. Chem. Phys.* 126:171102

69. Tikhonov AM. 2007. Compact layer of alkali ions at the surface of colloidal silica. *J. Phys. Chem. C* 111:930–37
70. Luo G, Malkova S, Pingali SV, Schultz DG, Schlossman ML, et al. 2005. X-ray studies of the interface between two polar liquids: neat and with electrolytes. *Faraday Discuss.* 129:23–34
71. Luo G, Malkova S, Yoon J, Schultz DG, Lin B, et al. 2006. Ion distributions at the nitrobenzene-water interface electrified by a common ion. *J. Electroanal. Chem.* 593:142–58
72. Lin B, Meron M, Gebhardt J, Graber T, Schlossman ML, Viccaro PJ. 2003. The liquid surface/interface spectrometer at ChemMatCARS synchrotron facility at the Advanced Photon Source. *Phys. B* 336:75–80
73. Schlossman ML, Synal D, Guan Y, Meron M, Shea-McCarthy G, et al. 1997. A synchrotron X-ray liquid surface spectrometer. *Rev. Sci. Instrum.* 68:4372–84
74. Born M, Wolf E. 1980. *Principles of Optics*. Oxford: Pergamon
75. Nevot L, Croce P. 1980. Characterization of surfaces by grazing X-ray reflection: application to the study of polishing of some silicate glasses. *Rev. Phys. Appl.* 15:761–80
76. Parratt LG. 1954. Surface studies of solids by total reflection of X-rays. *Phys. Rev.* 95:359–69
77. Tidswell IM, Ocko BM, Pershan PS, Wasserman SR, Whitesides GM, Axe JD. 1990. X-ray specular reflection studies of silicon coated by organic monolayers (alkylsiloxanes). *Phys. Rev. B* 41:1111–28
78. Schwickert H, Strobl G, Kimmig M. 1991. Molecular dynamics in perfluoro-*n*-eicosane. I. Solid phase behavior and crystal structures. *J. Chem. Phys.* 95:2800–6
79. Small DM. 1986. *The Physical Chemistry of Lipids*. New York: Plenum
80. Marcelja S. 1974. Chain ordering in liquid crystals. II. Structure of bilayer membranes. *Biochim. Biophys. Acta* 367:165–76
81. Defay R, Prigogine I, Bellemans A, Everett DH. 1966. *Surface Tension and Adsorption*. London: Longmans, Green & Co.
82. Marchenko VI. 1986. On the domain structure of two-dimensional ferromagnets. *J. Exp. Theor. Phys.* 63:1315–18
83. Andelman D, Brochard F, Joanny J-F. 1987. Phase transitions in Langmuir monolayers of polar molecules. *J. Chem. Phys.* 86:3673–81
84. Archer AJ, Wilding NB. 2007. Phase behavior of a fluid with competing attractive and repulsive interactions. arXiv:0706.0618v1
85. Takata Y, Murakami R, Taura J, Maki T, Mitsutake K, et al. 2002. Thermodynamic study on the adsorption of oleyl alcohol at oil/water interface. *Langmuir* 18:7544–48
86. Jang SS, Lin S-T, Maiti PK, Blanco M, Goddard WA. 2004. Molecular dynamics study of a surfactant-mediated decane-water interface: effect of molecular architecture of alkyl benzene sulfonate. *J. Phys. Chem. B* 108:12130–40
87. Panhuis MIH, Karaborni S. 1999. Simulating adsorbed layers of surfactant mixtures at an oil-water interface. *Philos. Mag. B* 79:9–14
88. Doe PH, Wade WH, Schechter RS. 1977. Alkyl benzene sulfonates for producing low interfacial tensions between hydrocarbons and water. *J. Colloid Interface Sci.* 59:525–31

89. Pautot S, Frisken BJ, Cheng J-X, Xie XS, Weitz DA. 2003. Spontaneous formation of lipid structures at oil/water/lipid interfaces. *Langmuir* 19:10281–87
90. Shchipunov YA. 1996. Liquid/liquid interfaces and self-organized assemblies of lecithin. In *Liquid-Liquid Interfaces Theory and Method*, ed. AG Volkov, DW Deamer, pp. 295–315. Boca Raton, FL: CRC
91. Zarbakhsh A, Querol A, Bowers J, Yaseen M, Lu JR, Webster JRP. 2005. Neutron reflection from the liquid-liquid interface: adsorption of hexadecylphosphorylcholine to the hexadecane-aqueous solution interface. *Langmuir* 21:11704–9
92. Varadaraj R, Brons C. 2007. Molecular origins of crude oil interfacial activity part 3: characterization of the complex fluid rag layer formed at crude oil-water interfaces. *Energy Fuels* 21:1617–21
93. Schlossman M. 2005. X-ray scattering from liquid-liquid interfaces. *Phys. B* 357:98–105